

Synchrotron X-ray studies of austenite and bainitic ferrite

BY H. J. STONE¹, M. J. PEET¹, H. K. D. H. BHADESHIA^{1,*},
P. J. WITHERS^{1,3}, S. S. BABU^{1,2} AND E. D. SPECHT^{1,4}

¹*Department of Materials Science and Metallurgy, University of Cambridge, Cambridge CB2 3QZ, UK*

²*Industrial, Welding and Systems Engineering, Ohio State University, Columbus, OH 43221, USA*

³*School of Materials, University of Manchester, Manchester M1 7HS, UK*

⁴*Oak Ridge National Laboratory, Oak Ridge, TN 37831, USA*

High-resolution synchrotron X-ray diffraction has been used to conduct *in situ* studies of the temporal evolution of phases during the isothermal growth of bainite. Two populations of austenitic material were identified: one corresponding to the initial austenite and the other to the carbon-enriched austenite associated with the bainitic ferrite. The observed lattice parameters and the asymmetry of the peaks from the residual austenite have been interpreted in terms of the carbon partitioning due to the transformation. The results are contrasted with an earlier study in which the austenite unit cell appeared to split into two distinct densities prior to the onset of transformation.

Keywords: bainite; austenite; synchrotron

1. Introduction

There is considerable interest in the atomic mechanism of the bainite transformation in steels, given the dramatic developments in the application of the phase in a variety of contexts (Abe 2004; Anon. 2004; DeCooman 2004; Jacques 2004; Klueh 2004; Yang & Fang 2005). There is also a demonstrated potential for major further developments (Caballero *et al.* 2001*a,b*, 2002; Garcia-Mateo *et al.* 2003*a,b*; Speer *et al.* 2004; Caballero & Bhadeshia 2004; Chatterjee *et al.* 2007). The topic has been the subject of intense research with the bainite transformation exposed to a variety of advanced experimental probes.

High-intensity X-ray experiments using synchrotron facilities are particularly interesting in this context. They enable accurate data such as lattice parameters, phase fractions and other details related to strain and homogeneity to be collected during the course of transformations in steels (Babu *et al.* 2002, 2005; Elmer *et al.* 2004).

One such study in which several of the present authors were involved (Babu *et al.* 2005) revealed a peculiar and as yet unexplained phenomenon—that the face-centred cubic (FCC) crystal structure of the parent austenite splits into

* Author for correspondence (hkdb@cam.ac.uk).

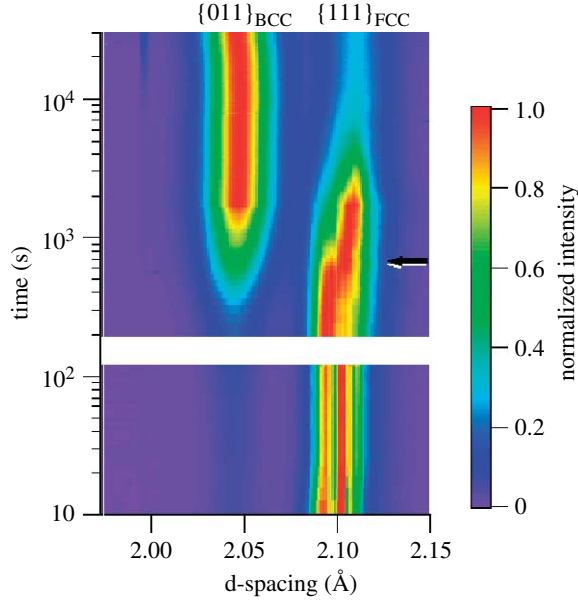


Figure 1. Diffraction data (Babu *et al.* 2005) showing in the lower part of the figure, that at small times before the onset of the bainite reaction, the austenite appears to have two different lattice parameters during isothermal holding at the transformation temperature. BCC, body-centred cubic.

two identical FCC lattices but with different lattice parameters *before* it begins to transform into bainite (figure 1). The experiments used an alloy in the Fe–0.8C–1.5Si–2Mn wt% system because the slow rate of reaction to bainite enables the experiment to be done easily. However, this alloy system is also an important one for study because the bainite transformation can be suppressed to temperatures as low as 125°C (Caballero *et al.* 2002). The result is an incredibly fine two-phase microstructure of just bainitic ferrite and carbon-enriched retained austenite—the plates of bainite are only 20–40 nm in thickness (Caballero *et al.* 2002; Brown & Baxter 2004; Bhadeshia 2005). This already has provided a viable production route to cheap, bulk nanostructured materials with an attractive combination of properties.

The purpose of the present work was therefore to investigate using the synchrotron facility at Grenoble, the kinetics of the transformation to nanostructured bainite with the simultaneous aim of studying further any precursor events in the parent austenite prior to transformation. The equipment used had a much higher resolution and a different detector system than that of the original Argonne experiments.

2. Experimental details

(a) Sample

An alloy, designated as alloy 1 (table 1) based on the Fe–0.8C–1.5Si–2Mn wt% system, was selected including additions of cobalt and aluminium. These additions are known to slightly accelerate the bainite reaction to enable

Table 1. Chemical compositions of alloys investigated in wt%.

alloy	Fe	C	Si	Mn	Mo	Cr	V	Co	Al
alloy 1	balance	0.79	1.56	1.98	0.24	1.01	—	1.51	1.01
alloy 2	balance	0.75	1.63	1.95	0.29	1.48	0.1	—	<0.01

experiments to be done in a reasonable time period consistent with synchrotron availability (Garcia-Mateo *et al.* 2003a). The alloy is also important from a technological perspective (Bhadeshia 2005) and is the main focus of the work reported here. A particular experiment needed to be conducted on alloy 2 (table 1), which is described towards the end of the paper. However, unless specifically mentioned, all the experiments and analyses refer to alloy 1.

Alloy 1 was homogenized for 48 h at 1200°C and transformed into bainite at 250°C. A cylindrical specimen 1.5 mm diameter by 5 mm long was cut from the previously transformed sample using electro-discharge machining followed by abrasion with a 400 grit SiC paper. With the 60 keV, X-rays used the signals originated from the entire thickness of the specimen rather than just the surface regions.

During the present synchrotron experiments (described later), the sample was austenitized at 832°C rather than at the 1000°C used in the original experiments (Babu *et al.* 2005). This leads to a reduction in the austenite grain size by a factor of approximately 2 (Garcia-Mateo *et al.* 2003a), which is useful in order to improve the counting statistics of integrated peak profiles. The fact that in the present work the whole sample volume is penetrated by the X-rays and that the sample is spun about its axis also helps in this respect.

(b) Synchrotron X-ray diffraction

The temporal evolution of phases during the bainite reaction was characterized *in situ* using synchrotron X-radiation and ID31 high-resolution powder diffractometer at the European Synchrotron Radiation Facility (ESRF) in Grenoble, France. Diffraction data are acquired using a nine-detector array. Each detector consists of a Si {111} analyser crystal and a Y–Al perovskite scintillator crystal viewed by a multi-stage photomultiplier tube. The individual detectors are separated by 2° in 2θ .

By sweeping this array through a range of 2θ greater than the angular separation of the individual detectors, overlapping frames of diffraction spectra are acquired from each detector. These are normalized according to the efficiency of each detector and averaged to generate a single diffraction pattern. The quality of the diffraction spectra obtained in this fashion may be improved by increasing the number of detectors that observe a given range of 2θ or by decreasing the scan rate. Where studies are performed on systems with a characteristic time comparable to that required to reliably acquire a spectrum, as in this study, compromises must be made on the degree of frame overlap and scan rates to ensure that the data are acquired with adequate time resolution.

A nominal incident beam energy of 60 keV was selected through diffraction from a double-crystal Si {111} monochromator. Initial calibration measurements were performed on Si and Na₂Ca₃Al₂F₁₄ (NAC) standard powders. Measurements were

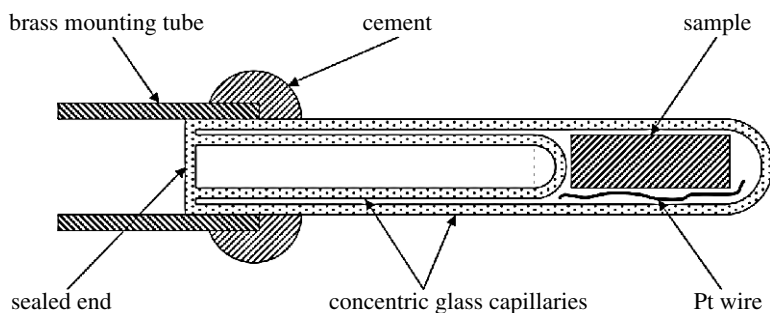


Figure 2. The sample assembly.

made scanning the central crystal of the array through $6^\circ \leq 2\theta \leq 30^\circ$ at 1° min^{-1} . Where frame overlap occurred, comparison of the diffraction signal recorded by each detector crystal allowed their relative efficiencies to be determined and hence enabled a normalization table to be obtained for subsequent measurements. From the diffraction data acquired with the Si powder standard, the wavelength of the incident beam was determined to be $0.20666 \pm 0.00001 \text{ \AA}$ from the measured positions of the first 10 peaks. The data acquired in these calibration measurements were also used for later analysis of peak shape to determine the resolution of the instrument in this configuration.

For temporal phase evolution measurements, only the central five crystals of the detector array were sufficient to capture the angular range of interest. For these measurements, the central crystal was scanned from $8.8^\circ \leq 2\theta \leq 11.0^\circ$ at 2° min^{-1} . This provided data from $4.8^\circ \leq 2\theta \leq 15.0^\circ$ from the central five crystals and had limited frame overlap. Acquisition times for each scan were 66 s after which 7 s were required to rotate the detector back to the start position.

During testing, the sample was located in a sealed glass capillary to avoid oxidation. A small piece of platinum wire alongside the sample provided a temperature reference via its lattice parameter and calibration data (figure 2). The sample assembly was spun at $3000g$ during diffraction to increase the population of grains contributing to the measured pattern and thereby improve the detected signal.

Two hot-air blowers were mounted on a translation stage directly beneath the sample assembly, with exit gas temperatures set to 1050°C (blower-A) and 350°C (blower-B), respectively, as determined by K-type thermocouples positioned at the mouth of each blower (figure 3). Subsequent comparison with data from the platinum wire indicated that the corresponding sample temperature when positioned above air blower-A was 832 ± 5 and $300 \pm 1^\circ\text{C}$ when positioned over air blower-B.

The sample was austenitized for approximately 30 min above air blower-A, while acquiring diffraction data to confirm full austenitization. Blower-B was then quickly (4.96 s) positioned beneath the sample by translation; the sample continued to glow at the point of entry into the cooler gas stream indicating that no significant undercooling occurred during the translation. In this position, diffraction data were acquired continuously until the bainite reaction was observed to cease. During this isothermal dwell, the sample temperature remained at 300.5°C with a s.d. of 1.3°C and maximum/minimum recorded excursions of $\pm 3^\circ\text{C}$.



Figure 3. Sample assembly mounted on the ID31 diffractometer hot-air blowers positioned underneath.

3. Results and discussion, alloy 1

(a) Instrumental resolution

The diffraction data acquired from the Si and NAC standard powders were partitioned into 0.0003° bins in 2θ . The peaks were fitted with a Voigt function (Langford 1978), implemented as a numerical convolution (Gold 1975) between normalized Gaussian and Lorentzian functions. This was further convolved with an axial divergence function (Finger *et al.* 1994), to account for the asymmetry of the peak arising as a result of finite detector and sample size.

Figure 4a shows that the width of the Gaussian component of the Voigt function for Si and NAC is on the same trend. This is expected since the Gaussian contribution to peak broadening arises predominantly from instrumental effects and is therefore sample independent. Furthermore, the data were readily fitted with a quadratic function in $\tan \theta$ (dashed line, figure 4a) consistent with the angular divergence associated with collimation for crystal spectrometers (Caglioti *et al.* 1958). In contrast, the Lorentzian components are different for the two powders, because they depend on sample characteristics such as particle size and heterogeneous strain (figure 4b). The success in reproducing the asymmetry of the peaks using the axial divergence function is illustrated in figure 4c,d.

If the Lorentzian component of the inherent instrumental resolution is taken as being at least as narrow as the data acquired from the NAC diffraction spectra, then the limiting angular separation of diffraction peaks to be separately resolved is approximately 0.0018° at $2\theta = 5.6^\circ$ —the lowest angle at which diffraction data are acquired. This corresponds to an equivalent separation of lattice plane spacing of 0.0003 \AA or a resolution of approximately 0.0005 \AA in the lattice parameter.

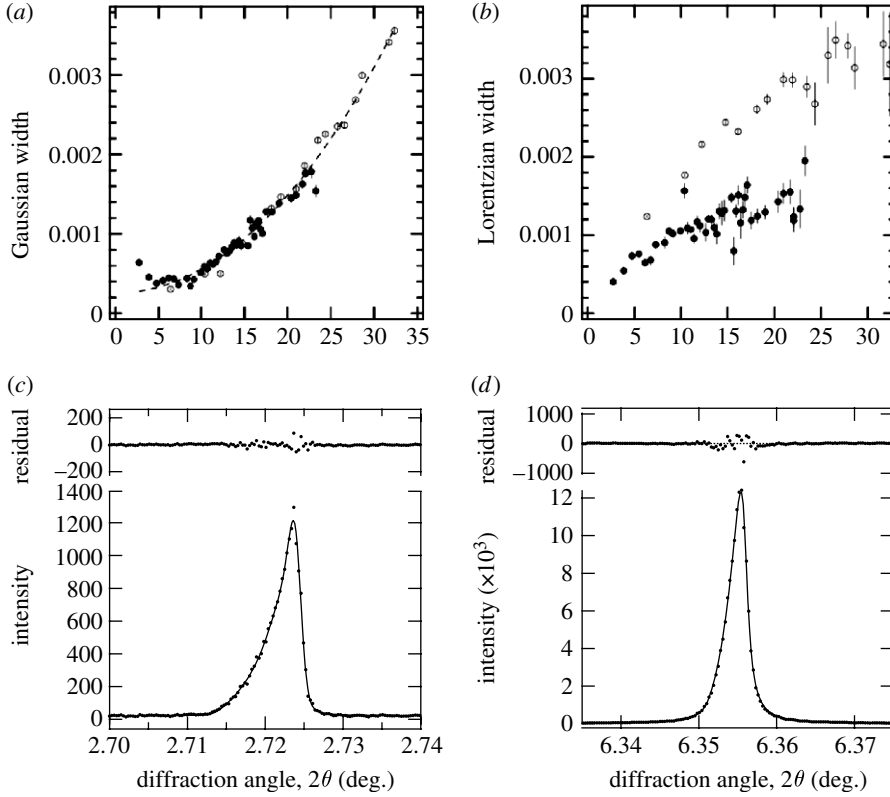


Figure 4. (a) Gaussian (filled circles, NAC; open circles, Si; dashed line, fit to data) and (b) Lorentzian widths (filled circles, NAC; open circles, Si) of the Voigt functions fitted to the individual peaks in the diffraction spectra obtained from the Si and NAC powders. (c,d) Illustrations of the excellent fit obtained with the asymmetric peaks of NAC and Si calibration samples after convolving with the axial divergence function.

(b) Evolution of spectra during transformation

The diffraction data obtained during transformation were partitioned into 0.002° bins in 2θ . No significant variations were observed on the time scale of individual scans (approx. 73 s). Subsequent analysis was therefore performed on datasets consisting of the sum of five consecutive scans to improve counting statistics.

Figure 5 shows examples from austenite $\{111\}$ and ferrite $\{110\}$ during transformation. The initial pattern consisted of narrow peaks exclusively from austenite. Their intensity decreased as transformation progressed. In addition, broad ferrite peaks appeared along with a second set of broad austenite peaks at lower 2θ angles than the initial ones. The latter is caused by the partitioning of carbon from the bainite into the residual austenite, thereby leading to an increase in its lattice parameter (Bhadeshia 2001). The partitioned carbon is heterogeneously distributed, leading to the two sets of austenite peaks (the enriched and unenriched austenite). This is also the reason why the intensity associated with the larger parameter (carbon-rich) austenite increases in parallel with that of bainitic ferrite.

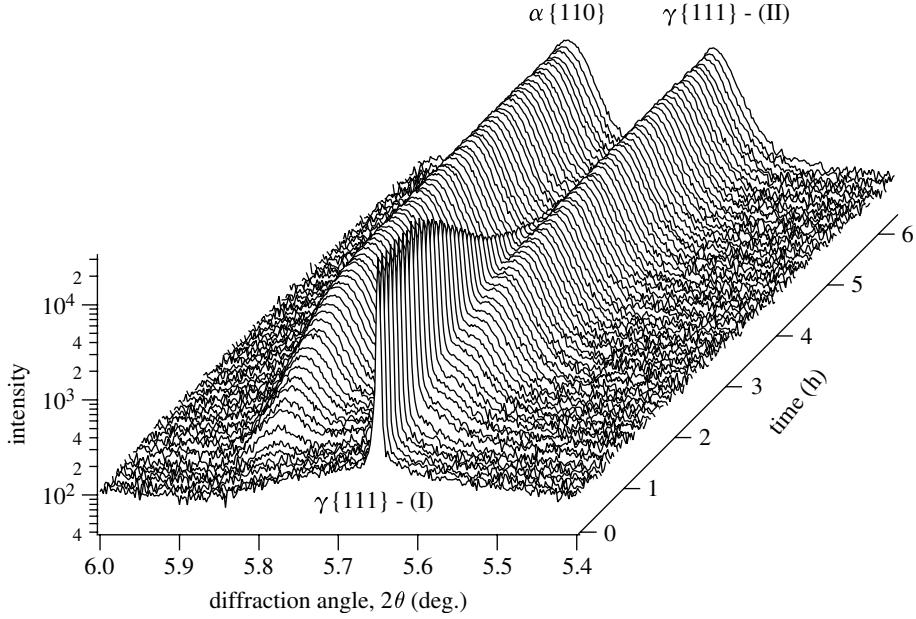


Figure 5. Austenite {111} and ferrite {110} peaks during isothermal heat treatment at 300°C following austenitization. Note that the intensity is plotted on a logarithmic scale.

The carbon concentration gradients, together with the non-uniform strains associated with the displacive formation of bainite, are responsible for the broad peaks following the commencement of transformation. The richest austenite is present as ‘films’ between platelets of bainitic ferrite, and the ‘blocks’ of austenite are those which are relatively poor in carbon (Matas & Hehemann 1961; Le-Houillier *et al.* 1971; Bhadeshia & Waugh 1982).

(c) Diffraction peak fitting

The bainitic ferrite peaks and the initial sharp austenite peaks were fitted with Voigt functions (Langford 1978) convolved with an axial divergence function (Finger *et al.* 1994) as described previously. However, the broadened secondary austenite peaks that accompany the development of the bainitic ferrite exhibited a further asymmetry, trailing towards low 2θ , which could not be adequately described in this way, but required a further convolution with an exponential function from zero to the peak position.

Examples of the fitted data obtained at a number of temperatures during the isothermal dwell at 300° are given in figure 6.

(d) Calculation of phase fractions

Phase fractions were determined from the diffracted intensities (I_0^{hkl}), accounting for the Lorentz polarization ($LP(\theta)$), the Debye–Waller factor ($\exp\{-2M\}$), the structure factor ($|F|^2$) and the multiplicities (p) of the individual peaks as follows:

$$I_0^{hkl} = I^{hkl} p |F|^2 \exp(-2M) LP(\theta), \quad (3.1)$$

where I^{hkl} is the absolute intensity.

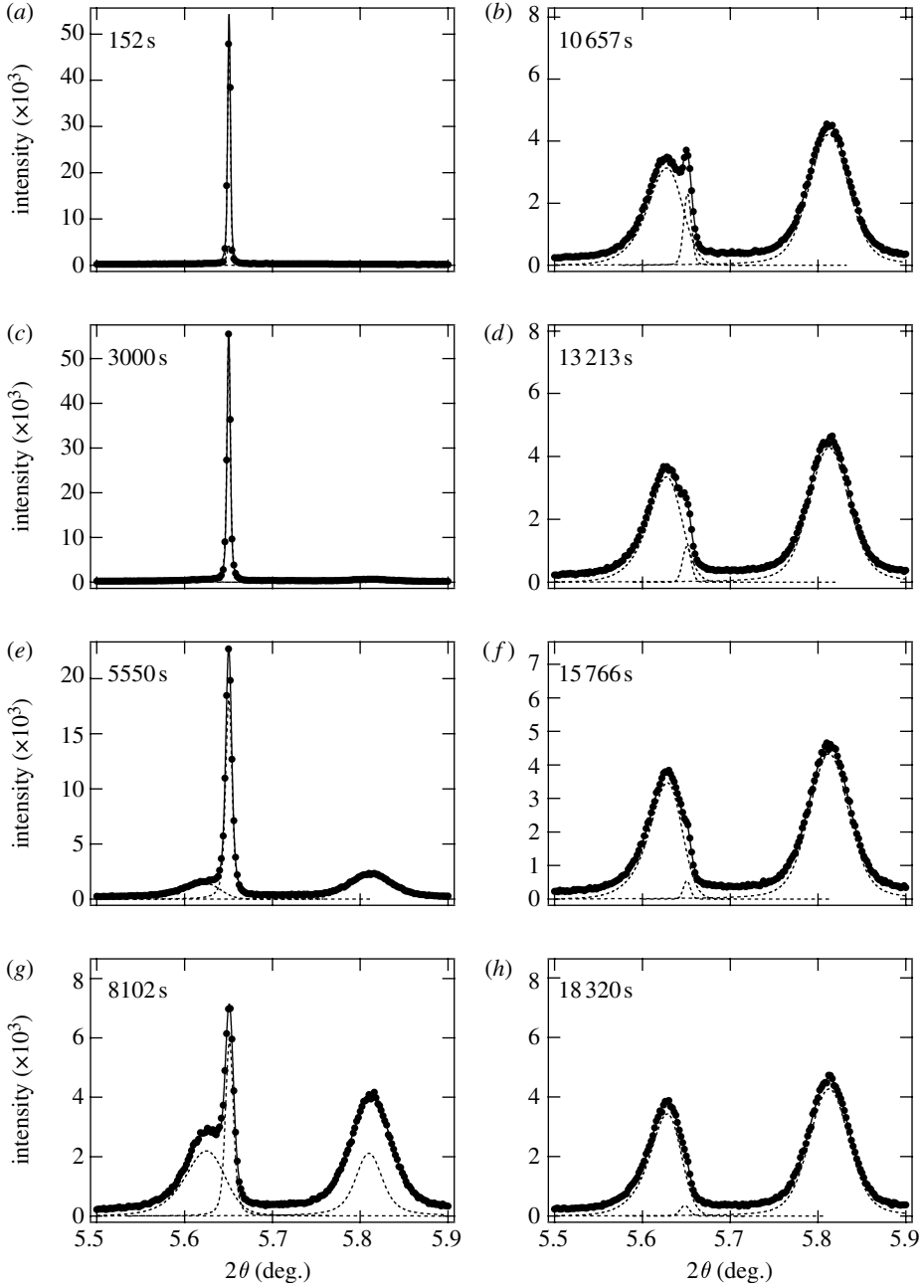


Figure 6. (a–h) Austenite {111} and ferrite {110} reflections during isothermal transformation. Solid lines represent the fit achieved; dotted lines represent the individual peak profiles less the background.

For austenite, $|F_\gamma|^2 = (4f)^2$, where f is the atomic scattering factor of an atom of iron. Similarly, $|F_\alpha|^2 = (2f)^2$.

As the synchrotron radiation is essentially fully polarized in the axial direction, there is no angular dependence of the polarization on the measured

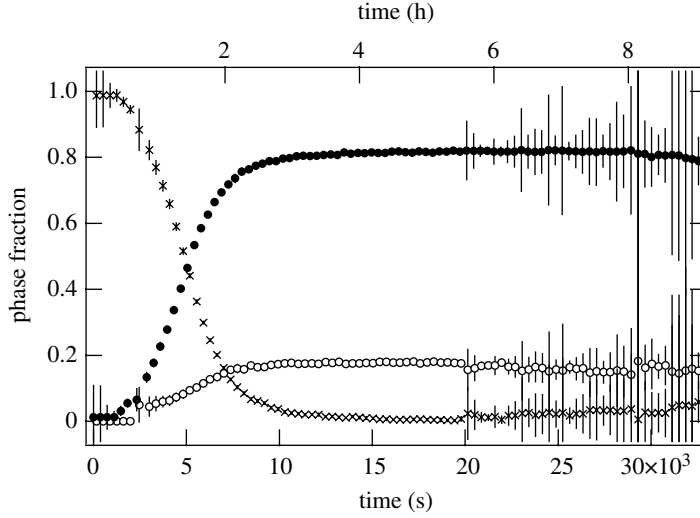


Figure 7. Fractions of the ferrite and both austenite populations during transformation at 300°C. The larger error bars towards the end of transformation come from the uncertainty in fitting the bulk austenite as its fraction tends towards zero. Uncertainty in the fitting of any peak reflects in all the others. The larger errors bars are therefore due to the fitting of the vanishing phase and do not provide a fair reflection of the actual uncertainty in the fractions of the film austenite and bainitic ferrite. Cross, bulk austenite; open circle, film austenite; filled circle, bainitic ferrite.

intensity, so the Lorentz polarization factor is simply $LP(\theta) = (\sin \theta \sin 2\theta)^{-1} = (2 \sin^2 \theta \cos \theta)^{-1}$.

In the Debye–Waller factor, $M = B(\sin \theta / \lambda)^2$, where $B = 8\pi^2 \langle \bar{u}_x^2 \rangle$ in which $\langle \bar{u}_x^2 \rangle$ is the time-averaged mean square displacement of scattering atom along the direction of the reciprocal lattice vector of the reflection hkl . If the vibrations are assumed to have spherical symmetry, this term does not vary with θ and may be assumed constant for a given temperature and material. Using the Debye approximation for this coefficient,

$$B = \frac{6h^2 T}{mk\Theta^2} \left(\frac{1}{x} \int_0^x \frac{\xi}{\exp(\xi) - 1} d\xi + \frac{x}{4} \right) \quad \text{where} \quad x = \frac{\Theta}{T}, \quad (3.2)$$

in which, h is Planck's constant, k is Boltzmann's constant, T is the sample temperature in Kelvin, m is the average atomic mass and Θ is the Debye temperature of the material.

Phase fractions were determined by taking the ratio of the corrected peak intensity for each species to the sum of all the peaks observed (figure 7).

Bainitic ferrite develops rapidly within the first few hours, reaching a final fraction of approximately 0.83. The proportion of film austenite increases simultaneously, maintaining a ratio of approximately 4.5 : 1 with the bainitic ferrite, reaching a final fraction of approximately 0.17. The bulk austenite at the same time tends towards zero. Consistent with the incomplete reaction phenomenon, the maximum fraction of bainite obtained is far less than expected from thermodynamic equilibrium (Bhadeshia & Edmonds 1979, 1980). The larger error bars at the end of the test (figure 7) are attributed to the difficulty in obtaining reliable fit in this region as the fraction of bulk austenite tends to be zero.

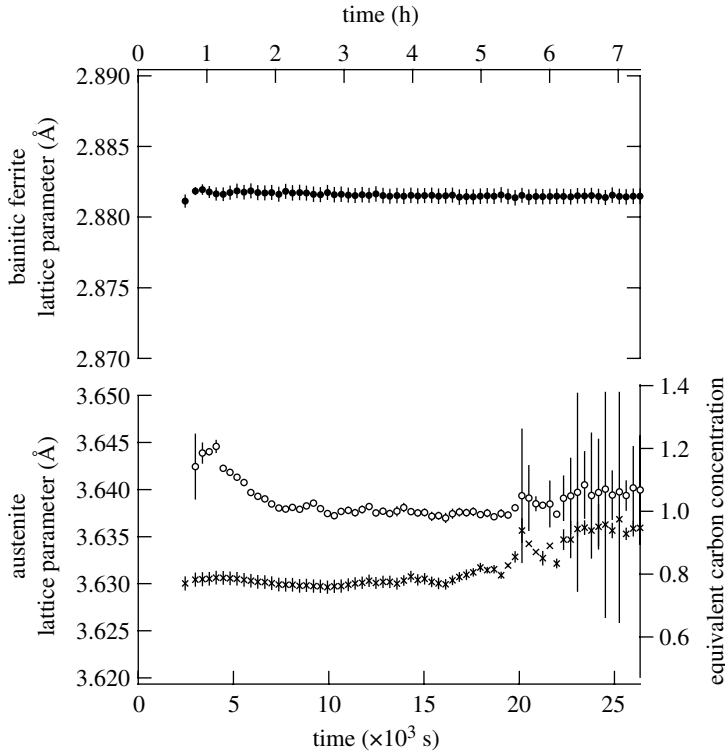


Figure 8. Lattice parameters of the bainitic ferrite and austenite populations during isothermal hold at 300°C after austenitization. The equivalent carbon concentrations for the two populations of austenite are also included. Cross, bulk austenite; open circle, film austenite; filled circle, bainitic ferrite.

During the early stages of transformation, the lattice parameter of the higher carbon films of austenite is greater than what it is towards the end of transformation as the carbon that is partitioned from the supersaturated ferrite diffuses over longer distances (figure 8). The carbon enrichment is greatest in the vicinity of the bainite plates, with distant blocky austenite affected little, thus giving rise to the bimodal austenite parameters (Bhadeshia & Edmonds 1979). The two values approach each other during the late stages of transformation as the blocky austenite itself diminishes in scale and evolves into films as the bainite penetrates it. The carbon concentrations of the two austenite regions (figure 8) are calculated from the lattice parameters assuming that the latter varies by $0.0330 \times \text{wt}\%$ of C (Dyson & Holmes 1970).

The carbon is not homogeneously distributed in the remaining austenite, localizing near the bainite plates where significant concentration gradients are expected (Mujahid & Bhadeshia 1992). These gradients may explain the asymmetry observed in the diffraction peaks associated with the carbon-rich regions of austenite. However, the degree of asymmetry of these peaks does not vary appreciably during the transformation to an extent that could be detected in the fitted peak profiles. It is therefore probable that the asymmetry arises as a result of differences in average carbon concentration of separate regions of austenite rather than local variations within individual regions; this is consistent

with high-resolution measurements of the carbon distribution (Self *et al.* 1981; Bhadeshia & Waugh 1982; Caballero *et al.* 2007). This is reasonable, as observations of this type of microstructure indicate that sheaves form with a significant variation in the size of austenite regions trapped between ferrite platelets (Chang & Bhadeshia 1995; §3e).

A similar, but much smaller, variation can be seen in the lattice parameter of the bainitic ferrite. During the period of more rapid transformation, the lattice parameter of the bainitic ferrite is observed to decrease from 2.8820 ± 0.0003 to 2.8814 ± 0.0005 Å. This variation is approximately 3.5 times greater than can be explained by the drift in sample temperature during isothermal transformation. Using the composition dependence of the lattice parameter in bainitic ferrite (Bhadeshia *et al.* 1991), this corresponds to a plausible change in the carbon content of bainitic ferrite by 0.013 wt%. Bainitic ferrite has been shown to contain excess carbon (Bhadeshia & Waugh 1982; Peet *et al.* 2004; Caballero *et al.* 2007) so that some redistribution is expected.

(e) *Microstructure*

The sample microstructure obtained after completion of the test using a JEOL 6340F FEGSEM following polishing and etching with nital is given in figure 9. It consists of bainitic ferrite and retained austenite, the latter in the form of films and blocks between the sheaves. No perceptible variations in the microstructure were observed across the sample or towards the surface; there were no signs of chemical segregation or decarburization. It is worth emphasizing that at 60 keV, the beam penetration is of the order of millimetres, so the results should not be sensitive to surface effects.

4. Comparison with previous work

Part of this work was inspired by the need to verify previous as yet unexplained observations that the austenite as a precursor to phase transformation decomposes into two-unit cells with different lattice parameters (Babu *et al.* 2005). The decomposition manifests as the splitting of X-diffraction peaks as illustrated in figure 1.

The resolution with which the present experiments have been conducted is approximately 20 times that of previous work. If peak splitting exists, then it can be detected with greater confidence. A trial split peak is illustrated in figure 10*a,d*, which is then convolved with the resolution function of the present (figure 10*b*) and previous (figure 10*e*) works, producing the expected outcomes as illustrated in figure 10*c,f*.

Figure 11 shows in a different format, and covering a broader range of Bragg angles, the same data as presented in figure 5. This is to emphasize that there is no austenite peak splitting to be seen before the onset of the bainite reaction. The question therefore remains as to why the earlier experiments contradict this conclusion.

One possibility is that the apparent splitting is an artefact introduced in the process of correcting the data for detector tilt and in the location of the centre of the pattern observed using the area detector (Babu *et al.* 2005). An example of the original raw data is presented in figure 12, representing the austenite prior to its transformation. It is a case in which the final plot in the form presented in

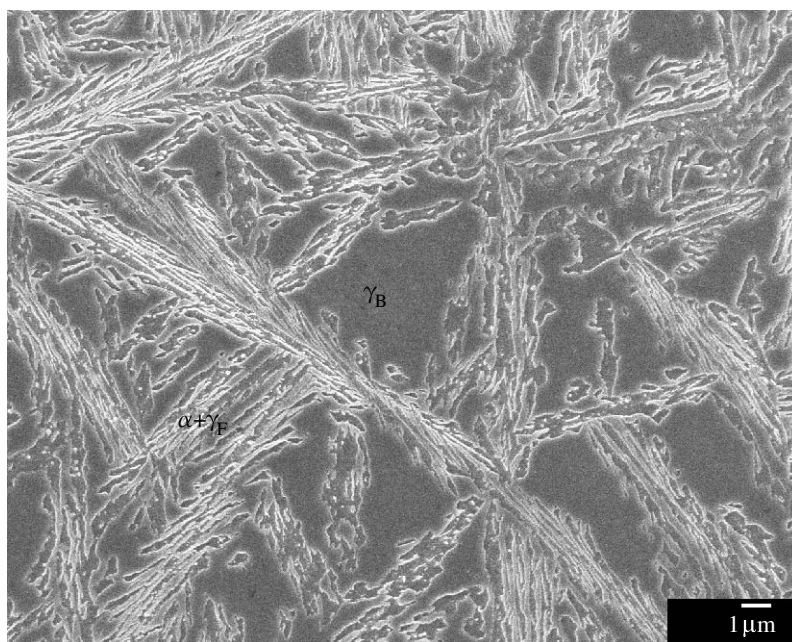


Figure 9. Microstructure after the cessation of isothermal transformation. γ_B represents the blocks of austenite, and $\alpha + \gamma_F$ the mixture of bainitic ferrite and films of austenite.

figure 1 revealed austenite peak splitting. It is clear however that the raw data do not, within the limits of resolution, show double rings associated with the expected locations of diffraction peaks from a single lattice. It is possible that within these limits, individual spots in an apparently single ring could originate from the crystals of austenite with unit cells of different densities. However, this would require an unlikely explanation of why the lattice parameter should vary between grains of austenite.

As figure 12 illustrates, there is a limited number of crystallites fulfilling the Bragg condition and contributing to the diffraction ‘rings’, making them spotty. When a ring consists mostly of a few strong and sharp reflections, integration will yield a peak profile dominated by those few peaks within the envelope of the instrumental resolution. Line shape analysis of the integrated profile then becomes unreliable.

For this reason, we have taken a set of data from similar experiments done on an Fe–Ni–C alloy where peak splitting has also been observed (Babu *et al.* 2007), and subjected it to analysis in which deliberate distortions are introduced during the integration of the diffraction rings into peaks, as illustrated in figure 13.

The integrated diffraction data obtained with optimal beam centre and tilt plane orientation angles are presented in figure 13a. This shows a single, approximately symmetric, narrow peak. By shifting the beam centre, 10 pixels in the horizontal direction from the optimal position, the peak displays pronounced asymmetry and appears to be composed of multiple sub-peaks (figure 13b). A similar degradation in the peak profile can also be obtained after integration with a 5° increase in the magnitude of the tilt of the detector.

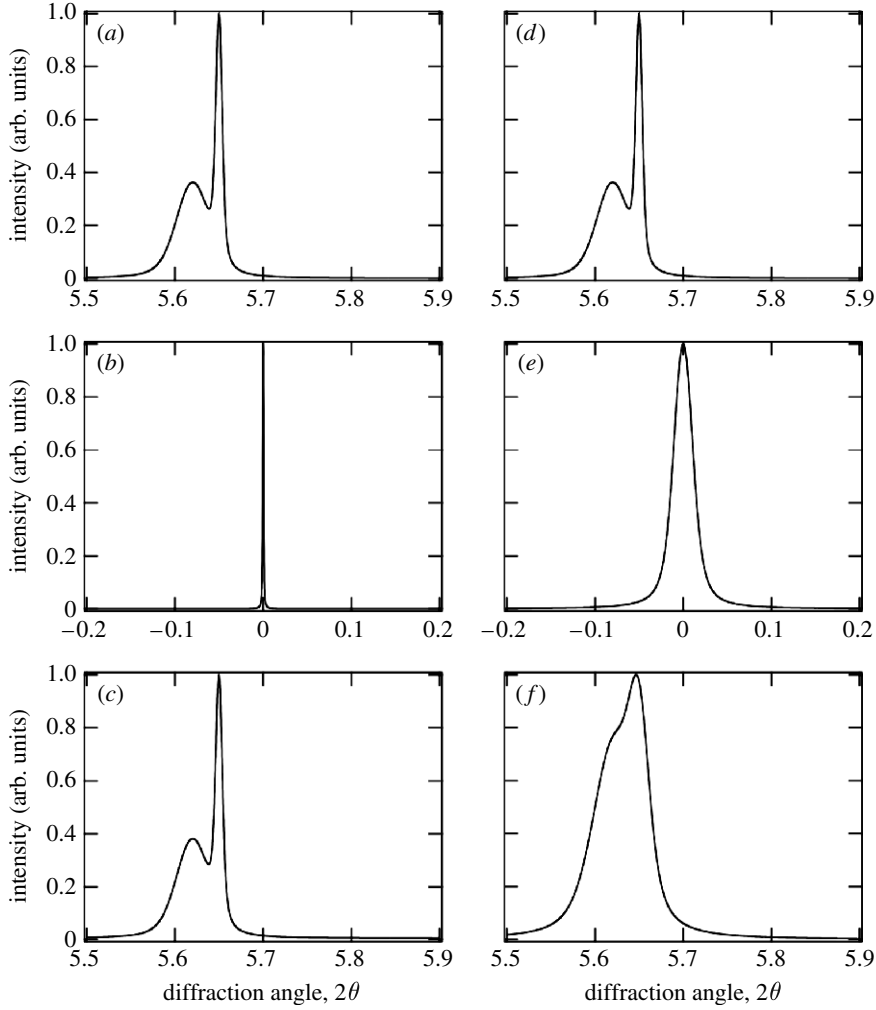


Figure 10. Simulation of the effect of resolution on observed data. (a,d) A perfect observation. (b,e) Estimated instrument resolution functions consistent with the resolution in the present and previous works, respectively. (c,f) The effect of convolving the ideal observation with the resolution.

Comparison of the detector beam centre and tilt angles used in the analysis of 59 studies on austenitic steel samples in earlier studies (E. D. Specht 2007, private communication) showed a variation in the beam centre in the horizontal direction with a s.d. of some two pixels and differences between the maximum and minimum of eight pixels. Similarly, the variation in the beam centre in the vertical direction had a s.d. of three pixels and differences between the maximum and minimum of 12 pixels. The magnitude of the tilt of the detector varied with a s.d. of approximately 1° with a difference between the maximum and minimum of 5° . As such, the degree of distortion artificially introduced in the analysis presented in figure 13 is consistent with the maximum likely to be seen in the experiments previously conducted and is likely to be larger than expected distortions by a factor of 3–5.

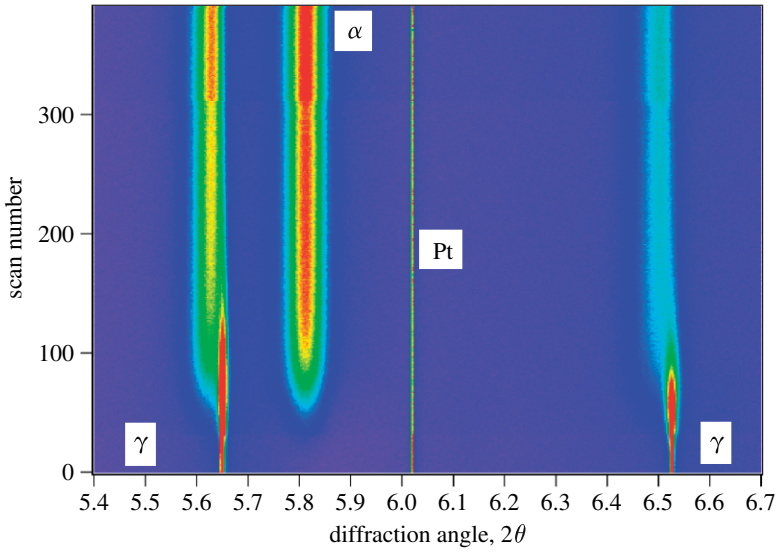


Figure 11. Isothermal diffraction scan data presented as a colour map showing austenite $\{111\}$ and ferrite $\{110\}$, Pt and austenite $\{002\}$ peaks during isothermal heat treatment at 300°C following austenitization.

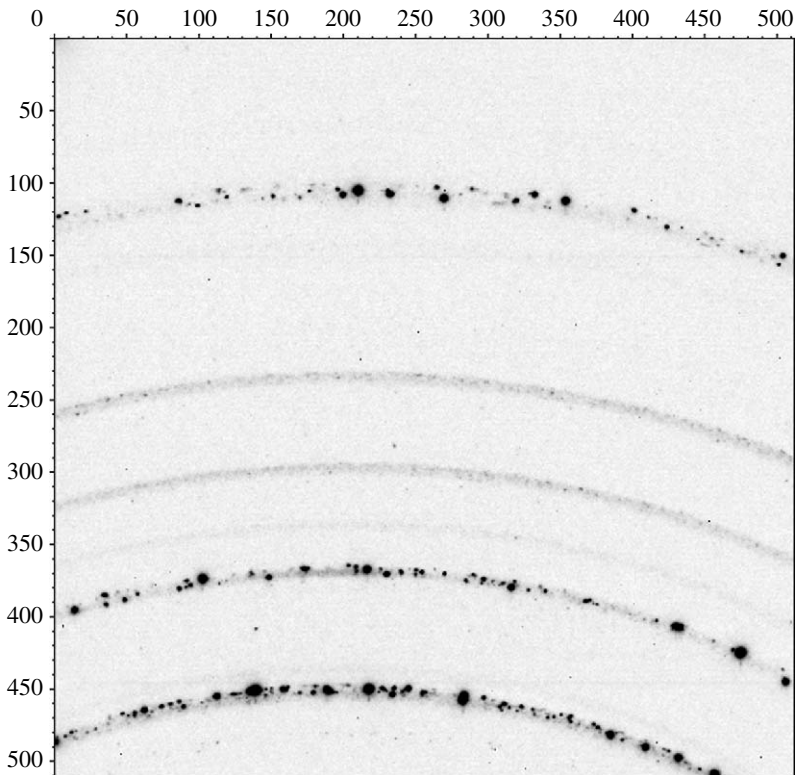


Figure 12. APS diffraction data from austenite prior to its transformation; starting from the bottom, the rings correspond to 111_γ , 002_γ , 224_M , 151_M , 404_M and 220_γ , where the subscript M refers to magnetite (Fe_3O_4 ; Babu *et al.* 2005).

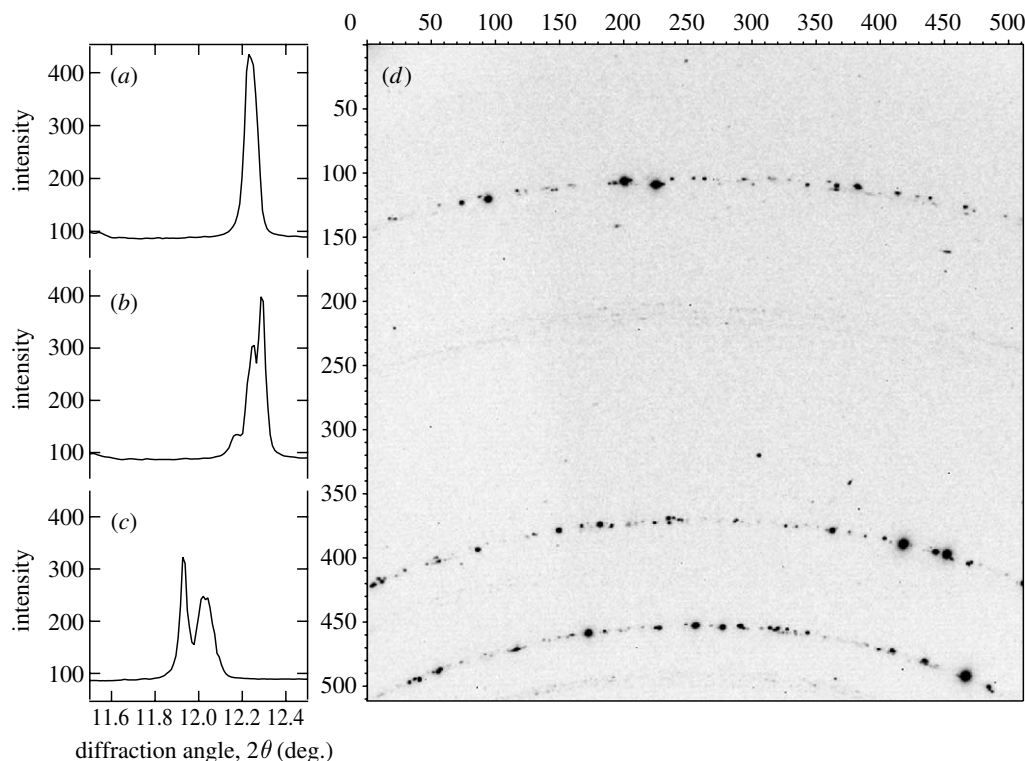


Figure 13. Analysis of the 111_{γ} data on Fe–Ni–C system (Babu *et al.* 2007). (a) A good integration. (b) With beam centre distortion. (c) With tilt distortion. (d) Data on which (a–c) are based (scales in pixels).

This analysis does, however, show that the integration procedure can introduce artefacts into the peak shape including asymmetries and doublets, which could be interpreted as peak splitting. Any peak that is genuinely split cannot be unsplit by introducing reasonable levels of tilt and centring errors; the fact that single peaks can be obtained (figure 13) strengthens the case for the absence of peak splitting in the original data.

5. Long-time experiment, alloy 2

Alloy 2 was used in our original experiments (Babu *et al.* 2005), which indicated precursor phenomena in the austenite. The isothermal transformation was conducted at 300°C in those experiments. One major advantage of this alloy is its very slow transformation rate at even lower temperatures (Caballero *et al.* 2002), permitting the state of the austenite to be studied without any possibility of interference from phase changes. We therefore conducted experiments on the austenite at 200°C, where the initiation of transformation takes days. The results are illustrated in figure 14 which clearly shows that there is no peak splitting in the austenite during approximately 10 hours at the transformation temperature.

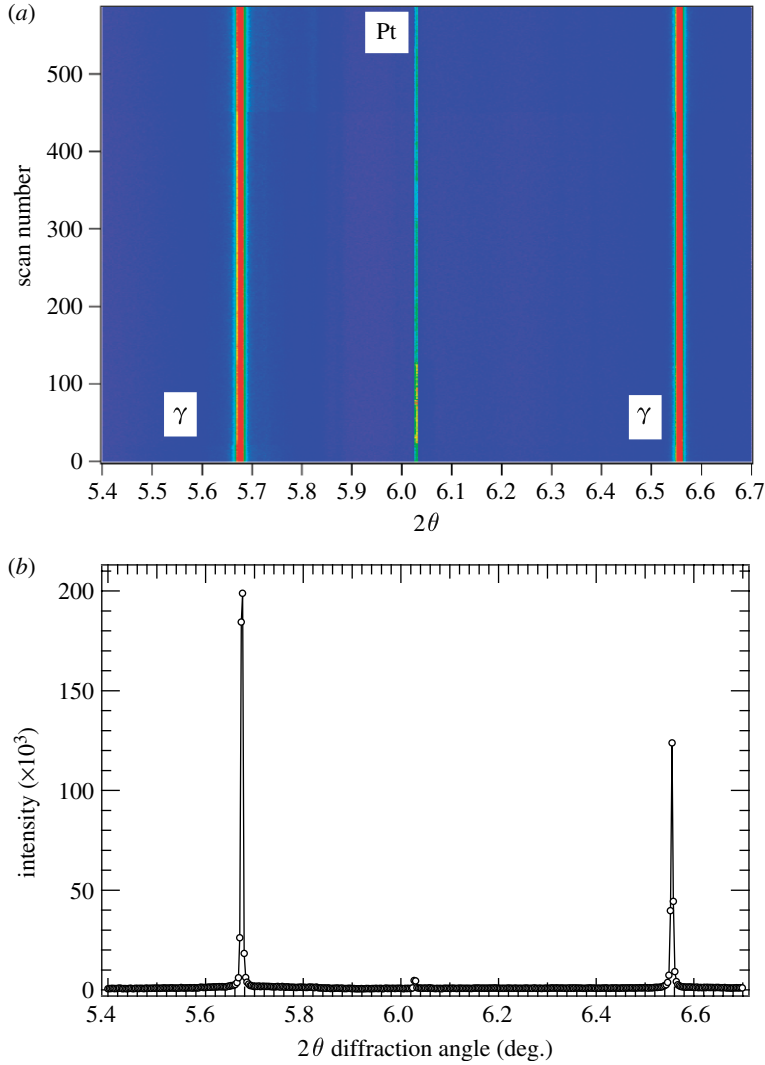


Figure 14. (a,b) Isothermal heat treatment of alloy 2 at 200°C showing a 10 hours span in which only austenite is present.

6. Conclusions

High-resolution diffraction indicates that two populations of austenite evolved during the course of transformation. One corresponds to the initial austenite, and the other to the carbon-enriched variety that remains untransformed between subunits of bainitic ferrite and between adjacent sheaves.

During the period of relatively rapid changes in volume fraction, the austenite richer in carbon (thin films) exhibits a larger lattice parameter than towards the end of reaction. This is consistent with the carbon partitioning behaviour.

The diffraction peaks associated with the austenite left after the formation of bainite exhibits an asymmetry that cannot be accounted for by instrumental

effects. This is attributed to a heterogeneous distribution of carbon in different regions of austenite because it takes time for carbon to homogenize after it is partitioned from supersaturated bainitic ferrite. The extent of asymmetry is constant during the course of transformation, indicating that there are separated regions of austenite with different carbon concentrations.

The high-resolution experiments reported here show that there is no division of austenite into two lattice parameter unit cells as a precursor to phase transformation during isothermal heat treatment. It is believed that previous much lower resolution experiments that contradict the present observations also do not show peak splitting when the raw data are reconsidered. It is probable that the integration of data introduces peak splitting as an artefact of analysis.

The present work proves that the austenite remains homogeneous prior to bainitic transformation, and that the reaction remains thermodynamically incomplete. The results therefore provide further support for a mechanism in which bainite growth is diffusionless, with carbon partitioning occurring subsequent to transformation (Ko & Cottrell 1952; Hehemann 1970; Bhadeshia & Edmonds 1979, 1980; Matsuzaki *et al.* 1994; Swallow & Bhadeshia 1996; Bhadeshia 2004; Chatterjee *et al.* 2006).

We are grateful to ESRF (Grenoble) for the synchrotron facilities and to the Engineering and Physical Sciences Research Council of the UK for funding the work on transformation plasticity, of which this work is a component. We acknowledge the support from the Division of Materials Sciences and Engineering, Office of Basic Energy Sciences, United States Department of Energy, under contract no. DE-AC05-00OR22725 with Oak Ridge National Laboratory, which is managed by UT-Battelle.

References

- Abe, F. 2004 Bainitic and martensitic creep-resistant steels. *Curr. Opin. Solid State Mater. Sci.* **8**, 305–311. (doi:10.1016/j.cossms.2004.12.001)
- Anon. 2004 ADI solutions aid vehicle design. *Foundary* **178**, 54–56.
- Babu, S. S., Elmer, J. W., David, S. A. & Quintana, M. A. 2002 *In situ* observations of non-equilibrium austenite formation during weld solidification of a Fe-C-Al-Mn low-alloy steel. *Proc. R. Soc. A* **458**, 811–821. (doi:10.1098/rspa.2001.0891)
- Babu, S. S., Specht, E. D., David, S. A., Karapetrova, E., Zschack, P., Peet, M. & Bhadeshia, H. K. D. H. 2005 *In-situ* observations of lattice parameter fluctuations in austenite and transformation to bainite. *Metall. Mater. Trans. A* **36**, 3281–3289. (doi:10.1007/s11661-005-0002-x)
- Babu, S. S., Specht, E. D., David, S. A., Karapetrova, E., Zschack, P., Peet, M. & Bhadeshia, H. K. D. H. 2007 Time-resolved X-ray diffraction investigation of austenite and transformation to bainite. In *First Int. Symp. on Steel Science* (eds K. Suzuki & T. Furuhashi), pp. 1–7. Tokyo, Japan: Iron and Steel Institute of Japan.
- Bhadeshia, H. K. D. H. 2001 *Bainite in steels*, 2nd edn. London, UK: Institute of Materials.
- Bhadeshia, H. K. D. H. 2004 Developments in martensitic and bainitic steels: role of the shape deformation. *Mater. Sci. Eng. A* **378**, 34–39. (doi:10.1016/j.msea.2003.10.328)
- Bhadeshia, H. K. D. H. 2005 Large chunks of very strong steel. *Mater. Sci. Technol.* **21**, 1293–1302. (doi:10.1179/174328405X63999)
- Bhadeshia, H. K. D. H. & Edmonds, D. V. 1979 The bainite transformation in a silicon steel. *Metall. Trans. A* **10**, 895–907. (doi:10.1007/BF02658309)
- Bhadeshia, H. K. D. H. & Edmonds, D. V. 1980 The mechanism of bainite formation in steels. *Acta Metall.* **28**, 1265–1273. (doi:10.1016/0001-6160(80)90082-6)

- Bhadeshia, H. K. D. H. & Waugh, A. R. 1982 Bainite: an atom probe study of the incomplete reaction phenomenon. *Acta Metall.* **30**, 775–784. (doi:10.1016/0001-6160(82)90075-X)
- Bhadeshia, H. K. D. H., David, S. A., Vitek, J. M. & Reed, R. W. 1991 Stress induced transformation to bainite in a Fe–Cr–Mo–C pressure vessel steel. *Mater. Sci. Technol.* **7**, 686–698.
- Brown, P. M. & Baxter, D. P. 2004 Hyper-strength bainitic steels. In *Materials science and technology 2004*, pp. 433–438. Warrendale, PA: TMS.
- Caballero, F. G. & Bhadeshia, H. K. D. H. 2004 Very strong bainite. *Curr. Opin. Solid State Mater. Sci.* **8**, 251–257. (doi:10.1016/j.cossms.2004.09.005)
- Caballero, F. G., Bhadeshia, H. K. D. H., Mawella, K. J. A., Jones, D. G. & Brown, P. 2001a Design of novel high-strength bainitic steels: part 1. *Mater. Sci. Technol.* **17**, 512–516.
- Caballero, F. G., Bhadeshia, H. K. D. H., Mawella, K. J. A., Jones, D. G. & Brown, P. 2001b Design of novel high-strength bainitic steels: part 2. *Mater. Sci. Technol.* **17**, 517–522.
- Caballero, F. G., Bhadeshia, H. K. D. H., Mawella, K. J. A., Jones, D. G. & Brown, P. 2002 Very strong, low-temperature bainite. *Mater. Sci. Technol.* **18**, 279–284. (doi:10.1179/026708301225000725)
- Caballero, F. G., Miller, M. K., Babu, S. S. & Garcia-Mateo, C. 2007 Atomic scale observations of bainite transformation in a high carbon high silicon steel. *Acta Mater.* **55**, 381–390. (doi:10.1016/j.actamat.2006.08.033)
- Caglioti, G., Paoletti, A. & Ricci, F. P. 1958 Choice of collimators for a crystal spectrometer for neutron diffraction. *Nucl. Instrum.* **3**, 223–228. (doi:10.1016/0369-643X(58)90029-X)
- Chang, L. C. & Bhadeshia, H. K. D. H. 1995 Austenite films in bainitic microstructures. *Mater. Sci. Technol.* **11**, 874–881.
- Chatterjee, S., Wang, H. S., Yang, J. R. & Bhadeshia, H. K. D. H. 2006 Mechanical stabilisation of austenite. *Mater. Sci. Technol.* **22**, 641–644. (doi:10.1179/174328406X86128)
- Chatterjee, S., Muruganath, M. & Bhadeshia, H. K. D. H. 2007 δ -TRIP steel. *Mater. Sci. Technol.* **23**, 819–827. (doi:10.1179/174328407X179746)
- DeCooman, B. 2004 Structure–properties relationship in TRIP steels containing carbide-free bainite. *Curr. Opin. Solid State Mater. Sci.* **8**, 285–303. (doi:10.1016/j.cossms.2004.10.002)
- Dyson, D. J. & Holmes, B. 1970 Effect of alloying additions on the lattice parameter austenite. *J. Iron Steel Inst.* **208**, 469–474.
- Elmer, J. W., Palmer, T. A., Babu, S. S., Zhang, W. & DebRoy, T. 2004 Direct observations of austenite, bainite, and martensite formation during arc welding of 1045 steel using time-resolved X-ray diffraction. *Weld. J. Res. Suppl.* **83**, 244s–253s.
- Finger, L. W., Cox, D. E. & Jephcoat, A. P. 1994 A correction for powder diffraction peak asymmetry due to axial divergence. *J. Appl. Crystallogr.* **27**, 892–900. (doi:10.1107/S0021889894004218)
- Garcia-Mateo, C., Caballero, F. G. & Bhadeshia, H. K. D. H. 2003a Acceleration of low-temperature bainite. *ISIJ Int.* **43**, 1821–1825.
- Garcia-Mateo, C., Caballero, F. G. & Bhadeshia, H. K. D. H. 2003b Development of hard bainite. *ISIJ Int.* **43**, 1238–1243.
- Gold, L. R. R. B. 1975 *Theory and application of digital signal processing*. Englewood Cliffs, NJ: Prentice-Hall.
- Hehemann, R. F. 1970 The bainite transformation. In *Phase transformations* (eds H. I. Aaronson & V. F. Zackay), pp. 397–432. Metals Park, OH: American Society for Metals.
- Jacques, P. J. 2004 Transformation-induced plasticity for high strength formable steels. *Curr. Opin. Solid State Mater. Sci.* **8**, 259–265. (doi:10.1016/j.cossms.2004.09.006)
- Klueh, R. L. 2004 Reduced-activation bainitic and martensitic steels for nuclear fusion applications. *Curr. Opin. Solid State Mater. Sci.* **8**, 239–250. (doi:10.1016/j.cossms.2004.09.004)
- Ko, T. & Cottrell, S. A. 1952 The formation of bainite. *J. Iron Steel Inst.* **172**, 307–313.
- Langford, J. I. 1978 A rapid method for analysing the breadths of diffraction spectral lines using the voigt function. *J. Appl. Crystall.* **11**, 10–14. (doi:10.1107/S0021889878012601)
- Le-Houillier, R., Begin, G. & Dube, A. 1971 A study of the peculiarities of austenite during the bainite transformation. *Metall. Trans.* **2**, 2645–2653.

- Matas, S. J. & Hehemann, R. F. 1961 The structure of bainite in hypoeutectoid steels. *TMS-AIME* **221**, 179–185.
- Matsuzaki, A., Bhadeshia, H. K. D. H. & Harada, H. 1994 Stress-affected bainitic transformation in a Fe–C–Si–Mn alloy. *Acta Metall. Mater.* **42**, 1081–1090. (doi:10.1016/0956-7151(94)90125-2)
- Mujahid, S. & Bhadeshia, H. K. D. H. 1992 Partitioning of carbon from supersaturated ferrite plates. *Acta Metall. Mater.* **40**, 389–396. (doi:10.1016/0956-7151(92)90313-4)
- Peet, M., Babu, S. S., Miller, M. K. & Bhadeshia, H. K. D. H. 2004 Three-dimensional atom probe analysis of carbon distribution in low-temperature bainite. *Scr. Mater.* **50**, 1277–1281. (doi:10.1016/j.scriptamat.2004.02.024)
- Self, P. G., Bhadeshia, H. K. D. H. & Stobbs, W. M. 1981 Lattice spacings from lattice fringes. *Ultramicroscopy* **6**, 29–40. (doi:10.1016/S0304-3991(81)80175-1)
- Speer, J. G., Edmonds, D. V., Rizzo, F. C. & Matlock, D. K. 2004 Partitioning of carbon from supersaturated plates of ferrite, with application to steel processing and fundamentals of the bainite transformation. *Curr. Opin. Solid State Mater. Sci.* **8**, 219–237. (doi:10.1016/j.cossms.2004.09.003)
- Swallow, E. & Bhadeshia, H. K. D. H. 1996 High resolution observations of displacements caused by bainitic transformation. *Mater. Sci. Technol.* **12**, 121–125.
- Yang, Z. G. & Fang, H. S. 2005 An overview on bainite formation in steels. *Curr. Opin. Solid State Mater. Sci.* **9**, 277–286. (doi:10.1016/j.cossms.2006.06.005)